SIAM J. NUMER. ANAL.
Vol. 60, No. 1, pp. 475–501

AN A POSTERIORI ERROR ESTIMATE OF THE OUTER NORMAL DERIVATIVE USING DUAL WEIGHTS*

SILVIA BERTOLUZZA†, ERIK BURMAN‡, AND CUIYU HE§

Abstract. We derive a residual based a posteriori error estimate for the outer normal flux of approximations to the diffusion problem with variable coefficient. By analyzing the solution of the adjoint problem, we show that error indicators in the bulk may be defined to be of higher order than those close to the boundary, which leads to more economic meshes. The theory is illustrated with some numerical examples.

Key words. a posteriori error estimate, normal flux, dual weighted residual method

AMS subject classifications. 65M50, 65M60

DOI. 10.1137/20M1358219

Let $\Omega \subset \mathbb{R}^d$, $d = 2, 3$, be a polygonal/polyhedral domain; let $\Gamma = \partial\Omega$ denote its boundary and ν the outer unit normal. We consider the following diffusion problem:

$$-\nabla \cdot a\nabla u = f, \text{ in } \Omega,$$

with nonhomogeneous Dirichlet boundary conditions, $u = g$ on Γ. The outer normal flux $\nu \cdot (a\nabla u)$ is an important quantity in many applications. It is of importance, for instance, when a heat flux or an electric field on the boundary of the domain needs to be approximated, or in fluid mechanics for the fluid forces [1, 29, 36, 20]. For boundary control problems, an accurate approximation of the normal flux on the boundary also plays a critical role [2, 3]. Recently there has been a number of works estimating the error for the outer normal flux in the a priori sense. We refer to [32, 35].

From the computational perspective it is appealing to apply adaptive methods that concentrate degrees of freedom where they are most needed to achieve a certain accuracy. In particular, for the normal flux on the boundary, we expect perturbations in the bulk of the domain to be less significant than those close to the boundary. This is proved in [14] where local a priori error estimates were given for the error in the outer normal flux. In particular, the error on the flux quantity was shown to depend on the H^1-error in a tubular neighborhood of the boundary and a global term that measures the global error in a weak norm. Similar results using boundary concentrated meshes were obtained more recently in [38], where the application to a Dirichlet boundary control problem was studied. A consequence of the localization property underlying the above a priori error estimates is that a standard energy norm estimate is unlikely to have optimal performance when approximating the normal flux, since it does not account for the relative independence of the goal quantity on perturbations in the

*Received by the editors August 10, 2020; accepted for publication (in revised form) October 22, 2021; published electronically February 22, 2022.
https://doi.org/10.1137/20M1358219
Funding: The work of the second and third authors was supported by the EPSRC grant EP/P01576X/1.
†Istituto di Matematica Applicata e Tecnologie Informatiche, IMATI-CNR, Pavia, PV, 27100, Italy (silvia.bertoluzza@imati.cnr.it).
‡Department of Mathematics, University College London, London, WC1E 6BT, UK (e.burman@ucl.ac.uk).
§School of Mathematical and Statistical Sciences, University of Texas Rio Grand Valley, Brownsville, TX 78520 USA (cuiyu.he@utrgv.edu).

bulk. It is, however, not straightforward to ensure accuracy of the boundary flux using a priori refinement in the boundary region alone, since geometric singularities or rough data nevertheless have to be taken into account.

The objective of the present work is to derive a residual based a posteriori error estimate for the outer normal flux that exploits the localization property. In particular, we add some mesh dependent weight in front of the classical residual based error estimator, and the weights greatly depend on the distance to the boundary. More precisely, the domain is implicitly divided into two zones, a tubular neighborhood around the boundary and an interior, bulk zone. For elements in the latter, the residual estimator is multiplied with the mesh diameter to a higher power than in the boundary region, hence giving it relative smaller weight. To get a precise quantification of the size of the weight we consider an adjoint problem. Thanks to suitable weighted estimates we determine the rate of the decrease of the adjoint solution and its derivatives with increasing distance to the boundary. This then helps provide bounds on the dual weights in the a posteriori error estimate that allow us to decompose the domain in a bulk and a boundary subdomain with associated error indicators.

The use of adjoint equations for the derivation of a posteriori error estimates in weak norms was first proposed by Eriksson and Johnson in [21] in the case of L^2 norm bounds. These ideas were generalized to the approximation of fluxes and fluid forces using the dual weighted residual a posteriori error estimation approach (see, for instance, [9, 10, 27, 8, 11, 39]). In these approaches, the dual solution was approximated, typically focusing on linear functionals of the error. There has recently been an increased interest in the convergence and optimality of goal oriented adaptive methods [5, 31, 24, 30, 7, 33, 6]. With this work we show that when the target quantity of the computation is the outward normal flux, a detailed analysis of the adjoint equation can lead to a posteriori bounds that perform better than the standard energy estimate but without the need of solving the dual problem numerically. Recall in this context that, when the target quantity driving the adaptive procedure is a norm of the error, the computation of the solution of the adjoint problem is complicated by the fact that the right-hand side depends on the error itself and is therefore not directly available, contrary to what happens, for instance, when the target quantity is a given known functional of the solution, such as the value at a point or the integral over a line.

Herein we only consider the standard finite element setting where the domain is meshed with a conforming triangulation. However, the arguments generalize in a straightforward manner to a posteriori error estimates for fictitious domain methods where elements are cut [17]. To extend the method to adaptive standard fictitious domain methods [28] in the spirit of [13], or domain decomposition methods, some more subtle arguments are needed. Indeed in such situations, the boundary divides the computational domain in two (or more) subdomains, thus requiring an analysis of the adjoint solution, similar to the one in this paper, for each subdomain and accounting for all boundaries and interfaces of the problem. This is the topic of a forthcoming paper.

An outline of the paper is as follows. First we introduce the weak formulation of our model problem and the associated finite element method in section 1. In section 2 we derive the a posteriori error estimate. Then we show in section 3 how to apply the results to some known stabilized methods, such as the Barbosa–Hughes methods and Nitsche's method. Finally, we illustrate the theory with some numerical examples in section 4.

1. The Lagrange multiplier formulation of the Dirichlet problem. For $g \in H^{1/2}(\Gamma)$ and $f \in L^2(\Omega)$ given, we consider the problem of finding $u \in H^1(\Omega)$, $\lambda \in H^{-1/2}(\Gamma)$ such that for all $v \in H^1(\Omega)$, $\mu \in H^{-1/2}(\Gamma)$,

$$\int_\Omega a\ \nabla u \cdot \nabla v - \int_\Gamma \lambda v = \int_\Omega f v, \qquad \int_\Gamma u\mu = \int_\Gamma g\mu, \tag{1.1}$$

where $a \in C^\infty(\bar{\Omega})$ is the diffusion coefficient, which for the sake of simplicity we assume to be scalar, satisfying $0 < \alpha \le a \le M$ for some constants α and M. We consider a Galerkin discretization of such problem. More precisely, letting $V_h \subset H^1(\Omega)$, $\Lambda_h \subset H^{-1/2}(\Gamma)$ be finite element spaces defined on a shape regular triangulation $\mathcal{T}_h$, we look for $u_h \in V_h$, $\lambda_h \in \Lambda_h$ such that for all $v_h \in V_h$, $\mu_h \in \Lambda_h$,

$$\int_\Omega a\,\nabla u_h \cdot \nabla v_h - \int_\Gamma \lambda_h v_h = \int_\Omega f v_h, \qquad \int_\Gamma u_h \mu_h = \int_\Gamma g\mu_h. \tag{1.2}$$

We assume that V_h contains the space of continuous piecewise polynomials of order k ($k \ge 0$) on $\mathcal{T}_h$, which we denote by $\breve{V}_h$, and that Λ_h contains a subspace $\breve{\Lambda}_h$ which is either the space of piecewise constants or the space of continuous piecewise linears on the mesh induced on Γ by $\mathcal{T}_h$.

Restricting the test functions in (1.1) to the discrete spaces and taking the difference of (1.1) and (1.2) we see that the following Galerkin orthogonality holds: for all $v_h \in V_h$, $\mu_h \in \Lambda_h$,

$$\int_\Omega a\ \nabla(u - u_h) \cdot \nabla v_h - \int_\Gamma (\lambda - \lambda_h) v_h = 0, \qquad \int_\Gamma (u - u_h)\mu_h = 0. \tag{1.3}$$

Observe that in the above we are as general as possible in the definition of the two spaces. We do not even need to assume that the spaces satisfy the inf-sup condition required for the stability of (1.2). This of course does not mean that the method is stable without it, only that the a posteriori error estimate will measure the computational error independently of the stability properties of the pair $V_h \times \Lambda_h$. An example of spaces that may be used in the framework is

$$V_h = \{u \in H^1(\Omega) :\ u|_T \in \mathbb{P}_k(T)\ \forall T \in \mathcal{T}_h\} \tag{1.4}$$

and, for $k' \ge 0$,

$$\Lambda_h = \{\lambda \in L^2(\Gamma) :\ u|_F \in \mathbb{P}_{k'}(F)\ \forall F \in \mathcal{T}_h|_\Gamma\} \tag{1.5}$$

or, for $k' \ge 1$,

$$\Lambda_h = \{\lambda \in C^0(\Gamma) :\ u|_F \in \mathbb{P}_{k'}(F)\ \forall F \in \mathcal{T}_h|_\Gamma\}. \tag{1.6}$$

Also variants of the spaces (1.5) and (1.6) with local conforming enrichment on the boundary to satisfy the inf-sup condition are valid [16].

Remark 1.1. We point out that, for $k' = k$, the choice (1.6) for the multiplier space, coupled with the choice (1.4) for the approximation of the primal unknown (i.e., choosing $\Lambda_h = V_h|_\Gamma$), yields a stable discretization of problem (1.1), equivalent to strongly imposing the Dirichlet boundary condition $u_h = \pi_h g$, where $\pi_h : L^2(\Gamma) \to V_h|_\Gamma$ is the $L^2(\Gamma)$ orthogonal projection. Then, using λ_h as an approximation to the normal flux is equivalent to computing the latter by postprocessing

with a variational approach as proposed, for instance, in [38]. Remark that, when the domain has corners, this method will not have, in general, optimal approximation for the multiplier, and it should be modified following the strategy used in the mortar method (see [12]), where discontinuity is allowed at the corners, with $k' = k - 1$ for those elements on the boundary mesh $\mathcal{T}_h|_\Gamma$ which are adjacent to the corners, and $k' = k$ for the remaining elements. Observe, however, that also for the suboptimal choice (1.6), the estimator we are going to present, remains valid.

2. A posteriori error estimates. The a posteriori error estimate is derived in three steps. We first derive an error representation using the adjoint problem. We then derive the local bounds for the adjoint solution, and, finally, we obtain the weighted residual estimates. In what follows we will use the notation $A \lesssim B$ to indicate that $A \le cB$ for some positive constant c independent of mesh size parameters such as element diameters and/or face diameters or edge lengths. $A \simeq B$ will stand for $A \lesssim B \lesssim A$.

2.1. Error representation using duality. We let

$$A : (H^1(\Omega) \times H^{-1/2}(\Gamma)) \times (H^1(\Omega) \times H^{-1/2}(\Gamma)) \to \mathbb{R}$$

be defined by

$$A(w, \eta; v, \zeta) = \int_\Omega a\, \nabla w \cdot \nabla v - \int_\Gamma \eta v + \int_\Gamma w\zeta. \tag{2.1}$$

Let $(u, \lambda) \in H^1(\Omega) \times H^{-1/2}(\Gamma)$ be the solution of (1.1), and let $(u_h, \lambda_h) \in V_h \times \Lambda_h$ satisfy (1.2). Set $e = u - u_h$ and $\delta = \lambda - \lambda_h$. We define $L : H^{-1/2}(\Gamma) \to \mathbb{R}$ as

$$L(\xi) := \|\delta\|^{-1}_{-1/2,\Gamma}(\delta, \xi)_{-1/2,\Gamma} \qquad \text{so that} \qquad L(\delta) = \|\delta\|_{-1/2,\Gamma},$$

where $(\cdot,\cdot)_{-1/2,\Gamma}$ is the scalar product for the space $H^{-1/2}(\Gamma)$, whose precise expression is provided later in (2.5), and where $\|\cdot\|_{-1/2,\Gamma}$ is the corresponding norm. Define $(z, \zeta) \in \mathcal{V} = H^1(\Omega) \times H^{-1/2}(\Gamma)$ as the solution of

$$A(w, \eta; z, \zeta) = L(\eta) \qquad \forall\ (w, \eta) \in \mathcal{V}. \tag{2.2}$$

Remark that the right-hand-side functional L depends on the unknown error δ, so that it is not possible to compute z, ζ, even only approximately. It is, however, easy to see that $|L(\xi)| \le \|\xi\|_{-1/2,\Gamma}$, and then the operator L has unitary norm. Therefore, by the stability of (2.2), we have

$$\|z\|_{1,\Omega} \lesssim 1, \qquad \|\zeta\|_{-1/2,\Gamma} \lesssim 1. \tag{2.3}$$

Let $\mathcal{F}_h^i$ and $\mathcal{F}_h^b$, respectively, denote the set of interior and boundary $(d-1)$-dimensional facets of the triangulation $\mathcal{T}_h$, and, for an element $T \in \mathcal{T}_h$, let ν_T denote the outer unit normal to ∂T. On a $(d-1)$-dimensional facet $F = \partial T^+ \cap \partial T^-$ we define the jump of the normal flux by $[\![a\, \partial_\nu u_h]\!] = a\, \nabla u_h^+ \cdot \nu_{T^+} + a\, \nabla u_h^- \cdot \nu_{T^-}$.

PROPOSITION 2.1 (error representation). *Let $\delta = \lambda - \lambda_h$, and let z, ζ be the solution of (2.2). Then it holds that for any $z_h \in V_h$ and $\zeta_h \in \Lambda_h$,*

$$\begin{aligned} \|\delta\|_{-1/2,\Gamma} = &\sum_{T\in\mathcal{T}_h} \int_T (f + \nabla \cdot a\, \nabla u_h)(z - z_h) - \sum_{F\in\mathcal{F}_h^i} \int_F [\![a\, \partial_\nu u_h]\!](z - z_h) \\ &+ \sum_{F\in\mathcal{F}_h^b} \int_F (\lambda_h - a\, \partial_\nu u_h)(z - z_h) + \int_\Gamma (g - u_h)(\zeta - \zeta_h). \end{aligned} \tag{2.4}$$

Proof. Taking $w = e$ and $\eta = \delta$ in (2.2) we have

$$\|\delta\|_{-1/2,\Gamma} = L(\delta) = A(e, \delta; z, \zeta).$$

Now, for $z_h \in V_h$, $\zeta_h \in \Lambda_h$ arbitrary, thanks to Galerkin orthogonality (1.3) we can write

$$\|\delta\|_{-1/2,\Gamma} = A(e, \delta; z - z_h, \zeta - \zeta_h) = I + II$$

with

$$I = \int_\Omega a\,\nabla e \cdot \nabla(z - z_h),\ II = -\int_\Gamma (a\,\partial_\nu u - \lambda_h)(z - z_h) + \int_\Gamma (g - u_h)(\zeta - \zeta_h).$$

For the term I we obtain using Green's theorem

$$\begin{aligned} I &= \int_\Omega a\,\nabla e \cdot \nabla(z - z_h) = \sum_{T\in\mathcal{T}_h} \int_T a\,\nabla e \cdot \nabla(z - z_h) \\ &= \sum_{T\in\mathcal{T}_h} \left(\int_T (f + \nabla \cdot a\,\nabla u_h)(z - z_h) + \int_{\partial T} a\,\nabla(u - u_h) \cdot \nu_T (z - z_h) \right) \\ &= \sum_{T\in\mathcal{T}_h} \int_T (f + \nabla \cdot a\,\nabla u_h)(z - z_h) - \sum_{F\in\mathcal{F}_h^i} \int_F [\![a\,\partial_\nu u_h]\!](z - z_h) \\ &\quad + \sum_{F\in\mathcal{F}_h^b} \int_F (a\,\partial_\nu u - a\,\partial_\nu u_h)(z - z_h). \end{aligned}$$

Combining all yields (2.4). This completes the proof of the proposition. ∎

2.1.1. Some observations on the operator L. We start by observing that taking $v_h = 1$ in (1.3) implies $\int_\Gamma \delta = 0$. Then we have

$$\|\delta\|_{-1/2,\Gamma} = \sup_{\phi\in H^{1/2}(\Gamma)} \frac{\int_\Gamma \delta\phi}{\|\phi\|_{1/2,\Gamma}} \simeq \sup_{\substack{\phi\in H^{1/2}(\Gamma) \\ \int_\Gamma \phi = 0}} \frac{\int_\Gamma \delta\phi}{|\phi|_{1/2,\Gamma}}.$$

On the space $H^{1/2}_\circ(\Gamma) = \{\phi \in H^{1/2} :\ \int_\Gamma \phi = 0\}$ of zero average functions in $H^{1/2}(\Gamma)$, we can define a scalar product and a norm, equivalent to the standard $H^{1/2}$ scalar product and norm, as

$$(\phi, \psi)_{1/2,\Gamma} = \int_\Omega \nabla\phi^{\mathcal{H}} \cdot \nabla\psi^{\mathcal{H}}, \qquad |\phi|_{1/2,\Gamma} := |\phi^{\mathcal{H}}|_{1,\Omega},$$

where $\phi^{\mathcal{H}} \in H^1(\Omega)$ denotes the harmonic lifting of ϕ. We then let $\|\cdot\|_{-1/2,\Gamma}$ be defined by duality with respect to the above norm. We now let $\mathfrak{R} : (H^{1/2}_\circ(\Gamma))' \to H^{1/2}_\circ(\Gamma)$ denote the Riesz isomorphism, which, we recall, is defined as the solution of

$$(\mathfrak{R}\lambda, \phi)_{1/2,\Gamma} = \int_\Gamma \lambda\phi \quad \forall\, \phi \in H^{1/2}_\circ(\Gamma).$$

We recall that, as $\mathfrak{R}$ is an isomorphism, we also have that

$$(\lambda, \mu)_{-1/2,\Gamma} = (\mathfrak{R}\lambda, \mathfrak{R}\mu)_{1/2,\Gamma} = \int_\Omega \nabla(\mathfrak{R}\lambda)^{\mathcal{H}} \cdot \nabla(\mathfrak{R}\mu)^{\mathcal{H}}. \tag{2.5}$$

It is now easy to check that, if $\mu \in L^2(\Gamma)$ satisfies $\int_\Gamma \mu = 0$, then $(\mathfrak{R}\mu)^{\mathcal{H}}$ is the unique solution of

$$-\Delta(\mathfrak{R}\mu)^{\mathcal{H}} = 0 \text{ in } \Omega, \qquad \int_\Gamma (\mathfrak{R}\mu)^{\mathcal{H}} = 0, \qquad \partial(\mathfrak{R}\mu)^{\mathcal{H}}/\partial\nu = \mu. \tag{2.6}$$

Indeed for any function $v \in H^1(\Omega)$, there is a unique decomposition $v = \bar{v} + v_1 + v_0$ such that $\bar{v} = |\Gamma|^{-1}\int_\Gamma v$, $v_0 \in H^{1/2}_\circ(\Gamma)$ is the harmonic extension of $v - \bar{v}$, and $v_1 \in H^1_0(\Omega)$ satisfies $\triangle v_1 = \triangle v$. Then we have that for any $v \in H^1(\Omega)$,

$$\int_\Omega \nabla(\mathfrak{R}\mu)^{\mathcal{H}} \cdot \nabla v = \int_\Omega \nabla(\mathfrak{R}\mu)^{\mathcal{H}} \cdot \nabla v_0 = (\mathfrak{R}\mu, v_0)_{1/2} = \int_\Gamma \mu v_0 = \int_\Gamma \mu v, \tag{2.7}$$

which is the weak form of (2.6).

2.2. Local estimates for the adjoint solution z. We observe that z is the solution of the following problem:

$$\int_\Omega a\,\nabla w \cdot \nabla z + \int_\Gamma w\zeta = 0, \qquad -\int_\Gamma \eta z = \|\delta\|^{-1}_{-1/2,\Gamma}(\delta,\eta)_{-1/2,\Gamma} = |\mathfrak{R}\delta|^{-1}_{1/2,\Gamma}\int_\Gamma \eta\,\mathfrak{R}\delta.$$

We rewrite this as

$$-\nabla \cdot a\,\nabla z = 0 \text{ in } \Omega, \qquad z = -|\mathfrak{R}\delta|^{-1}_{1/2,\Gamma}\mathfrak{R}\delta \text{ on } \Gamma.$$

The following lemma, whose proof we include for the sake of completeness, was proven in [34].

LEMMA 2.2. *Let $d_\Gamma(x)$ denote the distance of x from Γ, and let $w \in H^1(\Omega)$ satisfy $\nabla \cdot a\,\nabla w = 0$ in Ω. Then, for all $p \geq 0$ it holds that*

$$\|d_\Gamma^{p+1}\nabla^{p+2}w\|_{0,\Omega} \lesssim |w|_{1,\Omega}. \tag{2.8}$$

Proof. We start by proving a local bound. Let B_R and B_{cR}, $0 < c < 1$, be two concentric balls of radius, respectively, R and cR, and assume that $w \in H^1(B_R)$ satisfies $\nabla \cdot a\,\nabla w = 0$ in B_R. Then, we claim that for all $p \geq 0$ it holds that

$$\|\nabla^{p+2}w\|_{0,B_{cR}} \lesssim R^{-p-1}\|\nabla w\|_{0,B_R} + R^{-p-2}\|w\|_{0,B_R}, \tag{2.9}$$

where the implicit constant in the inequality depends on c. We start by proving (2.9) for $R = 1$. We prove it by induction on p. For $p = 0$, this is a consequence of [26, Theorem 8.8]. Let us now assume that the result is true for all $p \leq n-1$ and prove it for $p = n$. We let $c' = 1 - (1-c)/2 = c/2 + 1/2$ and let $\omega_c \in C^\infty_0(B_{c'})$, $\omega_c \geq 0$, $\omega_c = 1$ in B_c. We have

$$\nabla \cdot a\,\nabla(\omega_c w) = 2a\nabla w \cdot \nabla\omega_c + aw\Delta\omega_c + w\nabla a \cdot \nabla\omega_c \quad \text{ in } B_{c'} \qquad \omega_c w = 0 \quad \text{ on } \partial B_{c'}.$$

Using standard results on the smoothness of the solution of elliptic equations (see [26]), by the induction assumption we have that

$$\begin{aligned}\|\nabla^{n+2}w\|_{0,B_c} &\leq \|\nabla^{n+2}(\omega_c w)\|_{0,B_{c'}} \lesssim \|2a\nabla w \cdot \nabla\omega_c + aw\Delta\omega_c + w\nabla a \cdot \nabla\omega_c\|_{n,B_{c'}} \\ &\lesssim \|\nabla w\|_{n,B_{c'}} + \|w\|_{n,B_{c'}} \lesssim \|w\|_{1,B_1},\end{aligned}$$

which proves our claim for $R = 1$. By rescaling we immediately obtain (2.9).

Let us now prove (2.8). We consider a covering of Ω, consisting of a countable collection of balls $B_i = B_{r_i}(x_i) \subset \Omega$, of center x_i and radius r_i, with $r_i = \tilde{c}d_\Gamma(x_i)$ for some fixed $0 < \tilde{c} < 1$, such that

1. there exist $N \in \mathbb{N}$ such that all $x \in \Omega$ belong to at most N balls B_i;
2. for some $0 < c < 1$ independent of i, letting $\widetilde{B}_i \subset\subset B_i$ denote the ball of center x_i and radius cr_i, it holds that $\Omega \subseteq \cup_i \widetilde{B}_i$.

(By the Besicovitch covering theorem, such a collection exists.) We observe that the relation between the radius of the balls in our covering and the distance of the centers from the boundary of the domain implies that for all i, $x \in \widetilde{B}_i$ implies $d_\Gamma(x) \simeq r_i$. Then, letting $w_i = |B_i|^{-1} \int_{B_i} w$ denote the average of w in B_i, using (2.9) and a Poincaré inequality, we can write

$$\begin{aligned}\|d_\Gamma^{p+1}\nabla^{p+2}w\|_{0,\Omega}^2 &\le \sum_i \|d_\Gamma^{p+1}\nabla^{p+2}w\|_{0,\widetilde{B}_i}^2 \lesssim \sum_i r_i^{2(p+1)}\|\nabla^{p+2}w\|_{0,\widetilde{B}_i}^2 \\ &\lesssim \sum_i r_i^{2(p+1)}\|\nabla^{p+2}(w-w_i)\|_{0,\widetilde{B}_i}^2 \lesssim \sum_i (|w-w_i|_{1,B_i}^2 + r_i^{-2}\|w-w_i\|_{0,B_i}^2) \\ &\lesssim \sum_i |w|_{1,B_i}^2 \lesssim |w|_{1,\Omega}^2,\end{aligned}$$

which concludes the proof. ∎

2.3. The a posteriori error estimator. Using the error representation of Proposition 2.1 and the local bounds for the adjoint solution stated in (2.8), we will now derive the a posteriori error estimation. Compared to the classical residual based error indicator, our local error indicators for each element/facet are additionally multiplied by local dual weights depending on the distance from the element/facet to the boundary. Let us first introduce some notations that will be useful for the bounds.

We let h_T (resp., h_F) denote the diameter of an element T (resp., of a $(d-1)$-dimensional facet F) in $\mathcal{T}_h$. For a given element $T \in \mathcal{T}_h$, Δ_T denotes the patch of elements that have at least a vertex in common with T. The distance of an element T to the boundary will be measured using $\rho_T = \min_{x\in\Delta_T} d_\Gamma(x)$. That is the shortest distance from the associated patch to the boundary.

We now let $\widehat{\Pi}_h : H^1(\Omega) \to \check{V}_h$ denote the Scott–Zhang projector, introduced in [40]. We recall that, for $1 \le m \le k+1$, it holds that

$$\|z - \widehat{\Pi}_h z\|_{0,T} + h_T|z - \widehat{\Pi}_h z|_{1,T} \lesssim h_T^m |z|_{m,\Delta_T}. \tag{2.10}$$

Using this bound for $m = 1$ and $m = k+1$ we have the following local interpolation bounds for the adjoint solution.

LEMMA 2.3. *Let $z_h = \widehat{\Pi}_h z$; then we have the following two bounds:*

$$\|z - z_h\|_{0,T} + h_T|z - z_h|_{1,T} \le C_1 h_T |z|_{1,\Delta_T},$$
$$\|z - z_h\|_{0,T} + h_T|z - z_h|_{1,T} \le C_2 h_T^{k+1}\rho_T^{-k}\|d_\Gamma^k\,\nabla^{k+1}z\|_{0,\Delta_T}.$$

The constants C_1 and C_2 depend on the shape regularity of the mesh.

Proof. The first inequality is immediate by (2.10) with $m = 1$. The second inequality trivially holds for T with Δ_T adjacent to the boundary (for which $\rho_T^{-k} = \infty$). For the elements for which Δ_T is interior to Ω, it follows by first applying (2.10) with $m = k+1$, then multiplying and dividing by d_Γ^k, and finally bounding $d_\Gamma^{-k} \le \rho_T^{-k}$:

$$\|z - z_h\|_{0,T} + h_T|z - z_h|_{1,T} \lesssim h_T^{k+1}|z|_{k+1,\Delta_T} \lesssim h_T^{k+1}\rho_T^{-k}|d_\Gamma^k z|_{k+1,\Delta_T}.$$ ∎

Let us at first assume that we have $g \in H^1(\Gamma)$. Under such an assumption we have the following theorem.

THEOREM 2.4. *Define the following local residuals:*

$$
\begin{aligned}
\mathbf{r}(T) &= h_T \|f + \nabla \cdot a\,\nabla u_h\|_{0,T} \quad \forall T \in \mathcal{T}_h,\\
\mathbf{r}_0(F) &= h_F^{1/2} \|[\![a\,\partial_\nu u_h]\!]\|_{0,F} \quad \forall F \in \mathcal{F}_h^i,\\
\mathbf{r}_1(F) &= h_F^{1/2} \|\lambda_h - a\,\partial_\nu u_h\|_{0,F} \quad \forall F \in \mathcal{F}_h^b,\\
\mathbf{r}_2(F) &= h_F^{1/2} |g - u_h|_{1,F} \quad \forall F \in \mathcal{F}_h^b.
\end{aligned} \tag{2.11}
$$

Then we have

$$
\|\lambda - \lambda_h\|_{-1/2,\Gamma} \lesssim \sqrt{\sum_{T\in\mathcal{T}_h} \varsigma_T^2 |\mathbf{r}(T)|^2 + \sum_{F\in\mathcal{F}_h^i} \varsigma_F^2 |\mathbf{r}_0(F)|^2 + \sum_{F\in\mathcal{F}_h^b} (|\mathbf{r}_1(F)|^2 + |\mathbf{r}_2(F)|^2)}, \tag{2.12}
$$

where the element and facet weights ς_T and ς_F are defined by

$$
\varsigma_T = \min\{C_1, C_2 h_T^k \rho_T^{-k}\}, \quad \varsigma_F = \min\{\varsigma_T, \varsigma_{T'}\} \text{ with } F = T \cap T'. \tag{2.13}
$$

Proof. Let us start by splitting $\mathcal{T}_h$ as the union of two disjoint sets

$$
\mathcal{T}_h^1 = \Big\{ T \in \mathcal{T}_h : C_1 |z|_{1,\Delta_T} \le C_2 h_T^k \rho_T^{-k} \|d_\Gamma^k \nabla^{k+1} z\|_{0,\Delta_T} \Big\}, \qquad \mathcal{T}_h^2 = \mathcal{T}_h \setminus \mathcal{T}_h^1.
$$

Setting $z_h = \widehat{\Pi}_h z$ and $\zeta_h = 0$ in the error representation of Proposition 2.1, we have

$$
\begin{aligned}
\|\delta\|_{-1/2,\Gamma} = &\sum_{T\in\mathcal{T}_h} \int_T (f + \nabla \cdot a\,\nabla u_h)(z - \widehat{\Pi}_h z) - \sum_{F\in\mathcal{F}_h^i} \int_F [\![a\,\partial_\nu u_h]\!](z - \widehat{\Pi}_h z)\\
&+ \sum_{F\in\mathcal{F}_h^b} \int_F (\lambda_h - a\,\partial_\nu u_h)(z - \widehat{\Pi}_h z) + \int_\Gamma (g - u_h)\zeta.
\end{aligned}
$$

Observe that Lemma 2.3 gives us two error estimates for $\|z - \widehat{\Pi}_h z\|_{0,T}$, and, depending on whether $T \in \mathcal{T}_h^1$ or $T \in \mathcal{T}_h^2$, we apply the best possible estimate. This yields

$$
\begin{aligned}
&\sum_{T\in\mathcal{T}_h} \int_T (f + \nabla \cdot a\,\nabla u_h)(z - \widehat{\Pi}_h z)\\
&\quad\lesssim \sum_{T\in\mathcal{T}_h^1} \|f + \nabla \cdot a\,\nabla u_h\|_{0,T} C_1 h_T |z|_{1,\Delta_T}\\
&\qquad + \sum_{T\in\mathcal{T}_h^2} \|f + \nabla \cdot a\,\nabla u_h\|_{0,T} C_2 h_T^k \rho_T^{-k} \|d_\Gamma^k \nabla^{k+1} z\|_{0,\Delta_T}\\
&\quad= \sum_{T\in\mathcal{T}_h^1} \varsigma_T \mathbf{r}(T) |z|_{1,\Delta_T} + \sum_{T\in\mathcal{T}_h^2} \varsigma_T \mathbf{r}(T) \|d_\Gamma^k \nabla^{k+1} z\|_{0,\Delta_T}\\
&\quad\le \sqrt{\sum_{T\in\mathcal{T}_h} \varsigma_T^2 |\mathbf{r}(T)|^2} \sqrt{\sum_{T\in\mathcal{T}_h^1} |z|_{1,\Delta_T}^2 + \sum_{T\in\mathcal{T}_h^2} \|d_\Gamma^k \nabla^{k+1} z\|_{0,\Delta_T}^2}.
\end{aligned}
$$

Applying Lemma 2.2 we have

$$
\sum_{T\in\mathcal{T}_h^1} |z|_{1,\Delta_T}^2 + \sum_{T\in\mathcal{T}_h^2} \|d_\Gamma^k \nabla^{k+1} z\|_{0,\Delta_T}^2 \lesssim \|z\|_{1,\Omega}^2 + \|d_\Gamma^k \nabla^{k+1} z\|_{0,\Omega}^2 \lesssim \|z\|_{1,\Omega} \lesssim 1,
$$

so that

$$\sum_{T\in\mathcal{T}_h}\int_T (f+\nabla\cdot a\,\nabla u_h)(z-\widehat{\Pi}_h z) \lesssim \sqrt{\sum_{T\in\mathcal{T}_h}\varsigma_T^2|\mathbf{r}(T)|^2}, \tag{2.14}$$

where the constant in the inequality depends on Ω and a.

A similar argument can be applied for interior facets. Letting $F\in\mathcal{F}_h^i$, $F\subset\partial T$, the standard bound holds,

$$\begin{aligned}&\int_F [\![a\,\partial_\nu u_h]\!](z-\widehat{\Pi}_h z) \le \|[\![a\,\partial_\nu u_h]\!]\|_{0,F}\|z-\widehat{\Pi}_h z\|_{0,F}\\ &\lesssim \|[\![a\,\partial_\nu u_h]\!]\|_{0,F}\left(h_T^{-1/2}\|z-\widehat{\Pi}_h z\|_{0,T}+h_T^{1/2}|z-\widehat{\Pi}_h z|_{1,T}\right)\le \|[\![a\,\partial_\nu u_h]\!]\|_{0,F}h_T^{1/2}C_1|z|_{1,\Delta_T},\end{aligned} \tag{2.15}$$

as well as the enhanced bound,

$$\int_F [\![a\,\partial_\nu u_h]\!](z-\widehat{\Pi}_h z) \le \|[\![a\,\partial_\nu u_h]\!]\|_{0,F}C_2 h_T^{k+1/2}\rho_T^{-k}\|d_\Gamma^k\nabla^{k+1}z\|_{0,\Delta_T}. \tag{2.16}$$

As for the cell contribution to the a posteriori estimate, we can retain, for each facet, the more favorable estimator depending on whether the facet F belongs to an element in $\mathcal{T}_h^1$ or in $\mathcal{T}_h^2$. By similar argument to the ones used for the element residual term, we have

$$-\sum_{F\in\mathcal{F}_h^i}\int_F [\![a\,\partial_\nu u_h]\!](z-\widehat{\Pi}_h z) \lesssim C(\Omega)\sqrt{\sum_{e\in\mathcal{F}_h^i}\varsigma_F^2|\mathbf{r}_0(F)|^2}. \tag{2.17}$$

The boundary terms are treated in the standard way for any $F\in\mathcal{F}_h^b$ and $F\subset\partial T$,

$$\int_F(\lambda_h - a\,\partial_\nu u_h)(z-\widehat{\Pi}_h z)\le\|\lambda_h-a\,\partial_\nu u_h\|_{0,F}\|z-\widehat{\Pi}_h z\|_{0,F}\lesssim\|\lambda_h-a\,\partial_\nu u_h\|_{0,F}h_F^{1/2}|z|_{1,\Delta_T}. \tag{2.18}$$

Therefore,

$$\begin{aligned}&\sum_{F\in\mathcal{F}_h^b}\int_F(\lambda_h - a\,\partial_\nu u_h)(z-\widehat{\Pi}_h z)\\ &\lesssim\left(\sum_{F\in\mathcal{F}_h^b}h_F\|\lambda_h - a\,\partial_\nu u_h\|_{0,F}^2\right)^{1/2}\|z\|_{1,\Omega}\le\left(\sum_{F\in\mathcal{F}_h^b}|\mathbf{r}_1(F)|^2\right)^{1/2}.\end{aligned} \tag{2.19}$$

By (2.3), the last term can be bounded as

$$\int_\Gamma(g-u_h)\zeta\le\|g-u_h\|_{1/2,\Gamma}\|\zeta\|_{-1/2,\Gamma}\lesssim\|g-u_h\|_{1/2,\Gamma}.$$

Finally, since $g-u_h$ is orthogonal to $\breve{\Lambda}_h\subseteq\Lambda_h$, we can use Lemma 3 of [15] to bound

$$\|g-u_h\|_{1/2,\Gamma}^2\lesssim\sum_{F\in\mathcal{F}_h^b}h_F|g-u_h|_{1,F}^2=\sum_{F\in\mathcal{F}_h^b}|\mathbf{r}_2(F)|^2. \tag{2.20}$$

Combining all gives (2.12). This completes the proof of the theorem. ∎

If $g \in H^1(\Gamma)$, it is, therefore, natural, for the Lagrangian multiplier method, to define the following error indicator η_T for each element $T \in \mathcal{T}_h$, and estimator η, as

$$\begin{aligned} \eta_T &= \sqrt{\varsigma_T^2 |\mathbf{r}(T)|^2 + \sum_{F \in \mathcal{F}_h^i \cap \partial T} \varsigma_F^2 |\mathbf{r}_0(F)|^2 + \sum_{F \in \mathcal{F}_h^b \cap \partial T} (|\mathbf{r}_1(F)|^2 + |\mathbf{r}_2(F)|^2)}, \\ \eta &= \sqrt{\sum_{T \in \mathcal{T}_h} \eta_T^2}. \end{aligned} \tag{2.21}$$

If g is not in $H^1(\Gamma)$, we cannot get the full localization (2.20) of the residual $g - u_h$ on Γ. We can, however, resort, for the two-dimensional case, to [22, Theorem 2.2] and, for the three-dimensional case, to [23, Lemma 3.1], which allows us to bound

$$\|g - u_h\|_{1/2,\Gamma}^2 \lesssim \sum_{P \in \mathcal{N}_h^b} |g - u_h|_{1/2,\Delta_P}^2,$$

where $\mathcal{N}_h^b$ is the set of nodes of the mesh $\mathcal{T}_h$ on Γ and where for $P \in \mathcal{N}_h^b$, $\Delta_P \subset \Gamma$ is the patch formed by the boundary facets sharing P as a vertex. For those patches Δ_P for which $g|_{\Delta_P} \in H^1(\Delta_P)$, $|g - u_h|_{1/2,\Delta_P}$ can be further bounded by $\sum_{F \subset \Delta_P} |\mathbf{r}_2(F)|^2$. For the remaining patches, the $H^{1/2}(\Delta_P)$ seminorm of the residual will have to be computed by evaluating the double integral involved in the definition of the fractional norm.

Remark 2.5. Note that, in the implementation of the method, we do not explicitly use the splitting $\mathcal{T}_h = \mathcal{T}_h^1 \cup \mathcal{T}_h^2$, which is only needed for the theoretical analysis. Remark also that, for the elements adjacent to Γ, for which $\rho_T^{-k} = \infty$, we always have $\varsigma_T = C_1$.

3. Application to stabilized methods for the imposition of boundary conditions. In engineering practice it is often advantageous to use a stabilized method instead of choosing the spaces so that the inf-sup condition is satisfied. In this section we show how the proposed framework can be adapted to two of the most well-known stabilized methods, namely, the Barbosa–Hughes method [4] and Nitsche's method [37]. We assume for the sake of simplicity that $g \in H^1(\Gamma)$. Both the final results and the arguments are in the same spirit as Theorem 2.4 above, and therefore we only give sketches of the proofs.

3.1. Indicators for the Barbosa–Hughes method. The Barbosa–Hughes discrete problem reads: find $u_h \in V_h$, $\lambda_h \in \Lambda_h$ such that for all $v_h \in V_h$, $\mu_h \in \Lambda_h$ it holds that

$$\int_\Omega a \nabla u_h \cdot \nabla v_h - \int_\Gamma \lambda_h v_h \pm \alpha \sum_{F \in \mathcal{F}_h^b} h_F \int_F (a \partial_\nu u_h - \lambda_h)(a \partial_\nu v_h) = \int_\Omega f v_h, \tag{3.1}$$

$$\int_\Gamma u_h \mu_h - \alpha \sum_{F \in \mathcal{F}_h^b} h_F \int_F (a \partial_\nu u_h - \lambda_h) \mu_h = \int_\Gamma g \mu_h. \tag{3.2}$$

Here we use $\pm$ in front of the stabilization term in (3.1) to indicate that the analysis applies to both the symmetric and antisymmetric version of the method. The functional L and z, ζ are defined as in the previous section. Similarly we have the following error representation by subtracting (3.1) and (3.2) from (1.1): for arbitrary $z_h \in V_h$ and $\zeta_h \in \Lambda_h$ it holds that

$$
\begin{aligned}
L(\delta) &= \int_\Omega a\,\nabla e\cdot\nabla z - \int_\Gamma \delta z + \int_\Gamma e\zeta \\
&= \int_\Omega a\,\nabla e\cdot\nabla(z-z_h) - \int_\Gamma \delta(z-z_h) + \int_\Gamma e(\zeta-\zeta_h) \\
&\quad + \int_\Omega a\,\nabla e\cdot\nabla z_h - \int_\Gamma \delta z_h + \int_\Gamma e\zeta_h \\
&= \int_\Omega a\,\nabla e\cdot\nabla(z-z_h) - \int_\Gamma \delta(z-z_h) + \int_\Gamma e(\zeta-\zeta_h) \\
&\quad - \alpha \sum_{F\in\mathcal{F}_h^b} h_F \int_F (a\,\partial_\nu u_h - \lambda_h)(\zeta_h \mp a\,\partial_\nu z_h).
\end{aligned}
$$

From Proposition 2.1, we have

$$
\begin{aligned}
L(\delta) &= \sum_{T\in\mathcal{T}_h}\int_T (f+\nabla\cdot a\,\nabla u_h)(z-z_h) - \sum_{F\in\mathcal{F}_h^i}\int_F [\![a\,\partial_\nu u_h]\!](z-z_h) \\
&\quad + \sum_{F\in\mathcal{F}_h^b}\int_F (\lambda_h - a\,\partial_\nu u_h)(z-z_h) \\
&\quad + \int_\Gamma (g-u_h)(\zeta-\zeta_h) - \alpha\sum_{F\in\mathcal{F}_h^b} h_F\int_F (a\,\partial_\nu u_h-\lambda_h)(\zeta_h\mp a\,\partial_\nu z_h).
\end{aligned}
\tag{3.3}
$$

We again set $z_h = \widehat{\Pi}_h z$, $\zeta_h = 0$. The first three terms in (3.3) can be bounded using (2.14), (2.17), and (2.19). However, for the fourth term in (3.3), contrary to the previous case, we do not have that $u_h - g$ is orthogonal to the multiplier space; therefore, (2.20) no longer holds. Instead we only have the following weaker bound [22, 23]. Recall that $\mathcal{N}_h^b$ denote the set of boundary vertices of the triangulation, and for each $P\in\mathcal{N}_h^b$ denote by $\Delta_P\subset\Gamma$ the patch formed by the boundary faces sharing P as a vertex. We have

$$
\|g-u_h\|_{1/2,\Gamma}^2 \lesssim \sum_{P\in\mathcal{N}_h^b} |u_h-g|_{1/2,\Delta_P}^2 + \sum_{F\in\mathcal{F}_h^b} h_F^{-1}\|u_h-g\|_{0,F}^2. \tag{3.4}
$$

We can further localize the term $|u_h-g|_{1/2,\Delta_P}^2$. In order to do so we add and subtract $g_h^P\in\check{V}_h|_{\Delta_P}$, where g_h^P is the $L^2(\Delta_P)$ projection onto the local space of continuous piecewise linears on the $(d-1)$-dimensional local mesh $\mathcal{T}_h|_{\Delta_P}$, yielding

$$
|g-u_h|_{1/2,\Delta_P}^2 \lesssim |u_h-g_h^P|_{1/2,\Delta_P}^2 + |g_h^P-g|_{1/2,\Delta_P}^2,
$$

which, combining with the inverse inequality, gives

$$
|u_h-g_h^P|_{1/2,\Delta_P}^2 \lesssim h_P^{-1}\|u_h-g_h^P\|_{0,\Delta_P}^2 \simeq \sum_{F\subseteq\Delta_P} h_F^{-1}\|u_h-g_h^P\|_{0,F}^2,
$$

where $h_P = \max_{F\in\Delta_P} h_F$ (remark that the shape regularity of the mesh implies that for all $F\subseteq\Delta_P$ we have $h_F\simeq h_P$). Thanks to the fact that $g-g_h^P$ is orthogonal to the continuous piecewise linear functions, we have

$$
|g_h^P-g|_{1/2,\Delta_P}^2 \lesssim \sum_{F\subseteq\Delta_P} h_F|g_h^P-g|_{1,F}^2.
$$

We also observe that, for P a vertex of F,

$$\|g-u_h\|_{0,F}^2 \lesssim \|g-g_h^P\|_{0,F}^2 + \|g_h^P-u_h\|_{0,F}^2 \lesssim \sum_{F\subseteq\Delta_P} h_F|g_h^P-g|_{1,F}^2 + \|u_h-g_h^P\|_{0,F}^2.$$

Combining these bounds we easily obtain

$$\begin{aligned}\int_\Gamma (g-u_h)\zeta &\le \|g-u_h\|_{1/2,\Gamma}\|\zeta\|_{-1/2,\Gamma} \lesssim \|g-u_h\|_{1/2,\Gamma}\\ &\lesssim \sqrt{\sum_{P\in\mathcal{N}_h^b}\sum_{F\subseteq\Delta_P}(h_F^{-1}\|u_h-g_h^P\|_{0,F}^2 + h_F|g_h^P-g|_{1,F}^2)}\\ &= \sqrt{\sum_{P\in\mathcal{N}_h^b}\sum_{F\subseteq\Delta_P}|\mathbf{r}(F,P)|^2},\end{aligned} \tag{3.5}$$

where, for P a vertex of $F\subset\mathcal{F}_h^b$, we define

$$\mathbf{r}(F,P) = \sqrt{h_F^{-1}\|u_h-g_h^P\|_{0,F}^2 + h_F|g_h^P-g|_{1,F}^2}\,.$$

Finally, we bound the additional term resulting from the stabilization, namely,

$$\begin{aligned}&\sum_{F\in\mathcal{F}_h^b} h_F\int_F (a\,\partial_\nu u_h-\lambda_h)(a\,\partial_\nu(\widehat{\Pi}_h z))\\ &\le \sqrt{\sum_{F\in\mathcal{F}_h^b} h_F\|a\,\nabla u_h\cdot\nu-\lambda_h\|_{0,F}^2}\sqrt{\sum_{F\in\mathcal{F}_h^b} h_F\|a\,\partial_\nu(\widehat{\Pi}_h z)\|_{0,F}^2}\\ &\lesssim \sqrt{\sum_{F\in\mathcal{F}_h^b} h_F\|a\,\partial_\nu u_h-\lambda_h\|_{0,F}^2}.\end{aligned} \tag{3.6}$$

The last bound derives from a standard trace inequality on the element T associated to the boundary face F followed by an inverse inequality and an H^1 stability bound for $\widehat{\Pi}_h$:

$$\begin{aligned}\|a\,\partial_\nu(\widehat{\Pi}_h z)\|_{0,F} &\lesssim \|\nabla(\widehat{\Pi}_h z)\|_{0,F} \lesssim h_T^{-1/2}\|\nabla(\widehat{\Pi}_h z)\|_{0,T} + h_T^{1/2}|\nabla(\widehat{\Pi}_h z)|_{1,T}\\ &\lesssim h_T^{-1/2}\|\nabla(\widehat{\Pi}_h z)\|_{0,T} \lesssim h_T^{-1/2}|z|_{1,\Delta_T},\end{aligned} \tag{3.7}$$

which, together with (2.3), yields

$$\sum_{F\in\mathcal{F}_h^b} h_F\|a\,\partial_\nu(\widehat{\Pi}_h z)\|_{0,F}^2 \lesssim \|z\|_{1,\Omega}^2 \lesssim 1.$$

We then have

$$\alpha\sum_{F\in\mathcal{F}_h^b} h_F\int_F (a\,\nabla u_h\cdot\nu-\lambda_h)(a\,\partial_\nu(\widehat{\Pi}_h z)) \lesssim \alpha\sqrt{\sum_{F\in\mathcal{F}_h^b}|\mathbf{r}_1(F)|^2}, \tag{3.8}$$

where, we recall, $\mathbf{r}_1(F) = h_F^{1/2}\|a\,\partial_\nu u_h-\lambda_h\|_{0,F}$.

Collecting the above bounds we obtain the a posteriori error estimate for the Barbosa–Hughes formulation (3.1)–(3.2):

$$\begin{aligned}\|\lambda-\lambda_h\|_{-1/2,\Gamma}^2 \lesssim{}& \sum_{T\in\mathcal{T}_h}\varsigma_T^2|\mathbf{r}(T)|^2 + \sum_{F\in\mathcal{F}_h^i}\varsigma_F^2|\mathbf{r}_0(F)|^2\\ &+(1+\alpha^2)\sum_{F\in\mathcal{F}_h^b}|\mathbf{r}_1(F)|^2 + \sum_{P\in\mathcal{N}_h^b}\sum_{F\subseteq\Delta_P}|\mathbf{r}(F,P)|^2.\end{aligned} \tag{3.9}$$

3.2. Indicators for Nitsche's method. Let us now consider Nitsche's method, which reads: find $u_h \in V_h$ such that for all $v_h \in V_h$, there holds

$$\begin{aligned}&\int_\Omega a\,\nabla u_h\cdot\nabla v_h - \int_\Gamma v_h(a\,\partial_\nu u_h) \pm \int_\Gamma u_h(a\,\partial_\nu v_h) + \gamma\sum_{F\in\mathcal{F}_h^b} h_F^{-1}\int_F u_h v_h\\ &= \int_\Omega f v_h \pm \int_\Gamma g(a\,\partial_\nu v_h) + \gamma\sum_{F\in\mathcal{F}_h^b} h_F^{-1}\int_F g v_h.\end{aligned} \tag{3.10}$$

Following the work of Stenberg [41], which focuses on the Poisson equation but which is easily adapted to (1.1), Nitsche's method is equivalent to a Barbosa–Hughes method with the choice $\Lambda_h = L^2(\Gamma)$. The solution u_h, λ_h of (3.1)–(3.2) with $\Lambda_h = L^2(\Gamma)$ verifies that u_h solves (3.10) with $\gamma = \alpha^{-1}$, and we have that, on $e \subset \Gamma$,

$$\lambda_h = a\,\partial_\nu u_h + \gamma h_F^{-1}(g - u_h). \tag{3.11}$$

Due to the equivalence, $L(\delta)$ has the same representation (3.3) with α replaced by γ^{-1}. With the same choice of z_h and ζ_h, the first and second terms can be bounded using (2.14) and (2.17), respectively. The fourth term $\int_\Gamma (g - u_h)\zeta$ can be bounded using (3.5). For the remaining terms, observe that

$$\mathbf{r}_1(F) = h_F^{1/2}\|\lambda_h - a\,\partial_\nu u_h\|_{0,F} = h_F^{1/2}\|\gamma h_F^{-1}(g - u_h)\|_{0,F} := \gamma\mathbf{r}_3(F)$$

with

$$\mathbf{r}_3(F) = h_F^{-1/2}\|u_h - g\|_{0,F},$$

which, combining with (2.19) and (3.8), yields

$$\begin{aligned}&\sum_{F\in\mathcal{F}_h^b}\int_F(\lambda_h - a\,\partial_\nu u_h)(z - \widehat{\Pi}_h z) \mp \gamma^{-1}\sum_{F\in\mathcal{F}_h^b} h_F\int_F (a\,\partial_\nu u_h - \lambda_h)(a\nabla(\widehat{\Pi}_h z)\cdot\nu)\\ &\quad\lesssim \sqrt{\sum_{F\in\mathcal{F}_h^b}(1+\gamma^2)|\mathbf{r}_3(F)|^2}.\end{aligned} \tag{3.12}$$

Collecting all, we obtain the following a posteriori error bound for the normal flux computed using Nitsche's method:

$$\begin{aligned}&\|a\,\partial_\nu u - \lambda_h\|_{-1/2,\Gamma}\\ &\lesssim \sqrt{\varsigma_T^2\sum_{T\in\mathcal{T}_h}|\mathbf{r}(T)|^2 + \sum_{F\in\mathcal{F}_h^i}\varsigma_F^2|\mathbf{r}_0(F)|^2 + \sum_{F\in\mathcal{F}_h^b}(1+\gamma^2)|\mathbf{r}_3(F)|^2 + \sum_{P\in\mathcal{N}_h^b}\sum_{F\subseteq\Delta_P}|\mathbf{r}(F,P)|^2},\end{aligned} \tag{3.13}$$

where λ_h is given in (3.11).

Similarly as in (2.21), we can define the corresponding error indicator η_T and η for the Barbosa–Hughes and Nitsche's methods.

4. Numerical experiments. In this section we demonstrate the performance of the proposed error estimator on some simple, yet significant, two-dimensional test cases. Firstly, we demonstrate the action of the weight ς_T defined in (2.13) in the

adaptive mesh refinement procedure independently of any particular problem. For simplicity, we fix $C_1 = 1$. In the computation, we approximate ρ_T by the following:

$$\rho_T \approx \min_{x \in \mathcal{N}_{\triangle_T}} d_\Gamma(x),$$

where $\mathcal{N}_{\triangle_T}$ is the set of all vertices on $\triangle_T$.

We start with a 4 by 4 initial triangular mesh on a unit square domain; see Figure 1(a). A total number of 7 refinement steps is performed, and the marking strategy identifies an element $K \in \mathcal{T}_h$ to be refined if

$$\varsigma_T > 0.5\varsigma_{T,max}, \quad \text{where } \varsigma_{T,max} = \max_{T \in \mathcal{T}_h} \varsigma_T.$$

Figure 1 shows the meshes at various steps with $k = 2$ and $C_2 = 1.0$. It is easy to observe that significantly more refinements are placed near the boundary. Further experiments also show that the refinements on the boundary become more dominant if we decrease the value of C_2 or increase the order of k.

Remark 4.1. We note that, while the precise value of the best constants C_1 and C_2 in Lemma 2.3 is not known, it is possible to give an estimate of the ratio C_2/C_1 in terms of the Poincaré constant for the patch Δ_T. Indeed, as $\widehat{\Pi}_h$ preserves polynomials of degree not greater than k, we can write

$$\|u - \widehat{\Pi}_h u\|_{0,T} + h_T \|u - \widehat{\Pi}_h u\|_{1,T} \leq C_1 h_T \inf_{p \in \mathbb{P}_k} |u - p|_{1,\Delta_T},$$

and then we can choose C_2 such that C_2/C_1 is the smallest constant $C_{k,\text{best}}$ for which

$$\inf_{p \in \mathbb{P}_k} |u - p|_{1,\Delta_T} \leq C_{k,\text{best}} h_T^k |u|_{k+1,\Delta_T}.$$

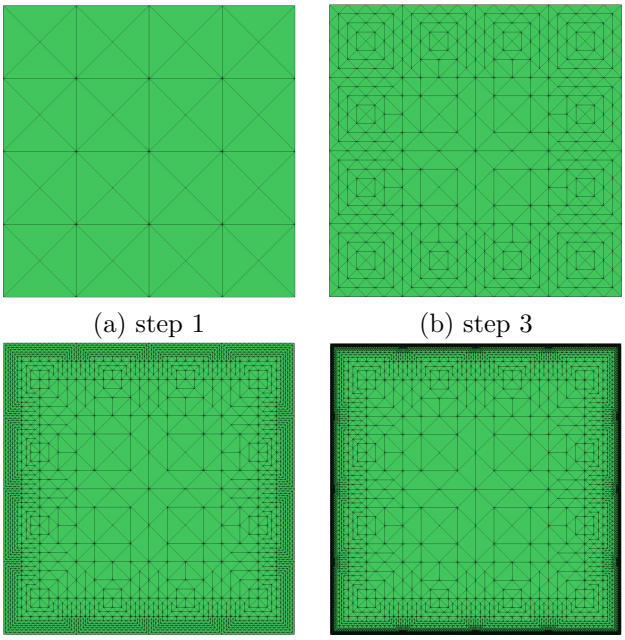

(a) step 1 (b) step 3

(c) step 5 (d) step 7

FIG. 1. *Adaptive meshes based on* ς_T *with* $k = 2$ *and* $C_2 = 1.0$.

Such a constant may be estimated by recursively applying some upper bound for the Poincaré constant for the patch Δ_T, which can be obtained, for instance, by the approach of [42]. Its dependence on the polynomial degree k can also be taken into account. For this choice to be the most effective, we would, however, need the upper bounds for $C_{k,\text{best}}$ to be sharp. If this is not the case, we observe that the true error might present some more or less pronounced oscillations. In our numerical tests, we tried several different values of C_2. In all the cases considered, setting C_2 between 0.1 and 1 turns out to be a reasonable choice. See also Remark 4.1.

4.1. Computation of the true error. In this subsection, we present two methods to compute the true error, i.e., $\|\lambda - \lambda_h\|_{-1/2,\Gamma}$, for the purpose of comparison. From (2.5) and (2.6),

$$\|\lambda - \lambda_h\|^2_{-1/2,\Gamma} = |\nabla w|^2_\Omega \quad (\text{or } \langle \lambda - \lambda_h, w\rangle_\Gamma),$$

where $w \in H^1(\Omega)$ satisfies the following variational problem:

$$\int_\Omega \nabla w \cdot \nabla v = \int_\Gamma (\lambda - \lambda_h) v \quad \text{and} \quad \int_\Gamma w = 0 \quad \forall\, v \in H^1(\Omega). \tag{4.1}$$

Note that (4.1) is a pure Neumann problem. The compatibility of the solution is guaranteed since $\int_\Gamma(\lambda - \lambda_h) = 0$ for all aforementioned numerical methods. We approximate the true error in each refinement step using a two order higher finite element method on a finer mesh (compared to the mesh used in the adaptive procedure). We let $w_h \in V_h^{k+2}$ denote the Galerkin projection of w on $V_h^{k+2} = \{v \in H^1(\Omega) : v|_T \in P^{k+2}(T) \quad \text{for all } T \in \tilde{\mathcal{T}}_h\}$. Here $\tilde{\mathcal{T}}_h$ is the finer mesh. We then approximate the error by

$$\|\lambda - \lambda_h\|^2_{-1/2,\Gamma} \approx |\nabla w_h|^2_\Omega \quad (\text{or } \int_\Gamma (\lambda - \lambda_h) w_h). \tag{4.2}$$

When λ does not have enough regularity, using (4.2) to accurately compute the true error becomes infeasible as a very fine mesh is required to guarantee the accuracy. We therefore introduce another method to compute the true error by exploring properties of the wavelet decomposition. Indeed, it is known that, by expanding a function in $H^{-1/2}(\Gamma)$ based on a suitable wavelet basis, an equivalent $H^{-1/2}(\Gamma)$ norm can be computed by taking a weighted L^2 norm of the coefficient vector. The latter can be efficiently computed by applying a wavelet transform [18]. This only requires computations on $\partial\Omega$; therefore, we are able to compute the true error to a satisfactory accuracy even for low regularity λ.

More precisely, given $v \in H^{-1/2}(\Gamma)$, we aim at computing $\|v\|_{-1/2,\Gamma}$. In order to do so, we consider the sequence of spaces $\{V_j\}_{j=0}^\infty$ such that $V_j \subset L^2(\Gamma)$ is the space of piecewise constant functions on the embedded uniform grid on Γ with mesh size $|\Gamma|2^{-j}$. We denote by $\{x_k^j\}_{k=0}^{2^j-1}$ the nodes of the corresponding mesh, which we assume to be ordered counterclockwise. For $v \in V_j$, we can compute the vector $\mathbf{v}_j$ of length 2^j:

$$\mathbf{v}_j := \{v_{jk}\}_{k=0}^{2^j-1} \quad \text{and} \quad v_{jk} = \frac{2^{j/2}}{|\Gamma|} \int_{x_k^j}^{x_{k+1}^j} v.$$

$\{v_{jk}\}_{k=0}^{2^j-1}$ is regarded as the coefficients of the $L^2(\Gamma)$ orthonormal bases consisting of the normalized characteristic functions on the elements of the grid. As $V_j \subset V_{j+1}$, for

all level j we can decompose $v_{j+1} \in V_{j+1}$ as $v_{j+1} = v_j + d_j$, with $v_j \in V_j$ obtained by applying a suitable oblique projector P_j to v_{j+1}. This gives us a telescopic expansion of all function in V_M as $v_M = v_0 + \sum_{j=0}^{M-1} d_j$ and, passing to the limit as M goes to infinity, of all functions in $L^2(\Gamma)$ as $v = v_0 + \sum_{j=0}^{\infty} d_j$. Given $\mathbf{v}_{j+1}$, we can compute $\mathbf{v}_j := \{v_{jk}\}_{k=0}^{2^j-1}$ and $\mathbf{d}_j := \{d_{jk}\}_{k=0}^{2^j-1}$ (this last one being the vector of coefficients of d_j with respect to a suitable basis for the space $W_j = (1 - P_j)V_{j+1}$) by applying a *low-pass filter* h (strictly related with the projector P_j) and the *band-pass filter* $g = [1, -1]$:

$$v_{jk} = \sum_{l=0}^{L} \frac{\sqrt{2}}{2} h(l)\, v_{j+1,2k+l} \quad \text{and} \quad d_{jk} = \sum_{l=0}^{1} \frac{\sqrt{2}}{2} g(l)\, v_{j+1,2k+l} = \frac{\sqrt{2}}{2} \left(v_{j+1,2k} - v_{j+1,2k+1}\right),$$

where $L + 1$ is the length of the low-pass filter h. In the above computation the function v is considered as periodic, so that, when the index $2k + l > 2^{j+1} - 1$, we extend the vector $\mathbf{v}_{j+1}$ as $v_{j+1,2^{j+1}+k} = v_{j+1,k}, k \geq 0$. For suitable choices of the low-pass filter h, the following norm equivalence holds for all $v \in H^{-1/2}(\Omega)$ [19]:

$$\|v\|^2_{-1/2,\Gamma} \simeq \|\mathbf{v}_0\|_2^2 + \sum_{j=0}^{\infty} 2^{-j} \|\mathbf{d}_j\|_2^2,$$

where $\|\cdot\|_2$ denotes the Euclidean norm. In our experiments we choose the so-called (2,2)-*biorthogonal wavelet* (see [18]), for which the low-pass filter h is

$$h = \frac{\sqrt{2}}{2}[3/128, -3/128, -11/64, 11/64, 1, 1, 11/64, -11/64, -3/128, 3/128].$$

By choosing M big enough and projecting v onto V_M (in our tests we use the L^2 orthogonal projection), we approximate the norm by

$$\|v\|^2_{-1/2,\partial\Omega} \approx \|\mathbf{v}_0\|_2^2 + \sum_{j=0}^{M-1} 2^{-j} \|\mathbf{d}_j\|_2^2. \tag{4.3}$$

4.2. Test results. Before presenting the results of our numerical tests, let us recall what the dependence of the error on the number of degrees of freedom is expected to be for an order k method on either a uniform or a boundary concentrated mesh: letting h denote the mesh size on the boundary and N the total number of degrees of freedom, we have $h \simeq N^{-1/2}$ for uniform meshes and $h \simeq N^{-1}|\log(N)|$ for boundary concentrated meshes. For a smooth solution, the error on the normal flux for optimal order k method will behave like h^k, that is, $N^{-k/2}$ for uniform grids and $N^{-k}|\log(N)|^k$ for boundary concentrated meshes.

To assess the performance of our estimator, we test it on the Lagrangian method without stabilization and on Nitsche's method (the Barbosa–Hughes method being equivalent to the latter). Nitsche's method with polynomial degree k is optimal, i.e., it yields an order k rate of convergence, on uniform meshes (see Table 1). For the Lagrangian method, the rate of convergence depends on the choice of the multiplier. We test two choices: discontinuous piecewise polynomials of order $k' = k - 2$ and continuous polynomials of order $k' = k$. Both choices yield inf-sup stable discretizations, yet they are both suboptimal (see Table 2): the first choice only provides, for

TABLE 1
Example 1*: Convergence rates for Nitsche's method on uniform meshes.*

	$k=1$				$k=2$			
h	E_1	rate	E_2	E_2/E_1	E_1	rate	E_2	E_2/E_1
1/8	3.35E-1	0.40	8.53E-2	0.25	2.86E-1	3.31	5.17E-2	0.18
1/16	1.73E-1	0.95	4.51E-2	0.26	3.19E-2	3.16	7.50E-3	0.23
1/32	8.66E-2	1.00	2.26E-2	0.25	4.69E-3	2.77	1.44E-3	0.30
1/64	4.33E-2	1.00	1.13E-2	0.26	2.51E-4	2.10	8.15E-5	0.32

TABLE 2
Example 1*: Convergence rates for Lagrangian multiplier method on uniform meshes.*

	$k=2,k'=0$				$k=2,k'=2$			
h	E_1	rate	E_2	E_2/E_1	E_1	rate	E_2	E_2/E_1
1/8	4.58E-2	1.88	1.14E-2	0.25	9.83E-3	2.67	3.13E-2	3.18
1/16	1.43E-2	1.68	3.97E-3	0.28	2.65E-3	1.89	7.74E-3	2.92
1/32	4.80E-3	1.57	1.40E-3	0.29	1.18E-3	1.15	2.60E-3	2.19
1/64	5.62E-4	1.54	1.82E-4	0.32	5.88E-4	1.01	1.15E-3	1.96

the normal flux, an approximation of order at most $k-1/2$, at the cost of using an order k method in the bulk, while, in the presence of corners, the second only allows for an order 1 approximation of the normal flux, independently of k, as it involves approximating a discontinuous function (the normal flux, in the presence of corners) by means of continuous functions. We point out that we are in no way advocating such choices as recommended methods for solving the problem considered (other choices for the multiplier—see Remark 1.1—allowing for optimality, are of course to be preferred for the actual computation of the flux). However, considering such suboptimal cases allows us to put the robustness of our method to the test and to show that the refinement driven by our estimator can somehow make up for the lack of optimality.

Example 1. In this example, we consider the Poisson equation on the unit square domain with right-hand side and boundary data chosen so that the solution is the Franke function [25]

$$\begin{aligned} u(x,y) = {} & 0.75\exp\left(-(9x-2)^2/4-(9y-2)^2/4\right) \\ & + 0.75\exp\left(-(9x+1)^2/49-(9y+1)/10\right) \\ & + 0.5\exp\left(-(9x-7)^2/4-(9y-3)^2/4\right) - 0.2\exp\left(-(9x-4)^2-(9y-7)^2\right). \end{aligned}$$

This function has two peaks at $(2/9,2/9)$ and $(7/9,1/3)$ and one sink at $(4/9,7/9)$.

We firstly test the convergence rate of the true error $\|\lambda-\lambda_h\|_{-1/2,\Gamma}$ on uniform meshes. The true error is computed using the aforementioned two methods. We denote by E_1 the error computed by (4.2) and by E_2 the error computed using the wavelet in (4.3) with $M=20$. The problem (4.2) is solved on a finer uniform mesh with mesh size $h=1/64$. Tables 1 and 2 show the convergence rates for E_1. Observe that these are in agreement with the expected convergence rates given by the standard error estimates for the two methods, that is, order 1 (resp., 2) for Nitsche's method with $k=1$ (resp., $k=2$) and order 3/2 (resp., 1) for the Lagrangian multiplier method with $k=2$, $k'=0$ (resp., $k=2$, $k'=2$). From Tables 1 and Table 2, we also observe that the ratio between E_2 and E_1 is relatively stable (the fluctuation of the ratio is likely caused by the inaccurate computation of E_1). In particular, for Nitsche's method, the ration E_2/E_1 remains close to 0.25 for both orders. These results, therefore, confirm that E_2 is equivalent to the true error for both the Nitsche and Lagrangian multiplier methods.

We now test the adaptive mesh refinement (AMR) procedure for the Lagrangian method. In the adaptive procedure, we set the stopping criteria such that the total number of degrees of freedom (DOFs) is less than $20,000$. The marking strategy is set such that an element T is marked to be refined if $\eta_K \geq 0.5\eta_{K,max}$. In this example, we set $C_2 = 1.0$. The initial mesh is set to be the 4×4 mesh in Figure 1(a). For comparison, we also perform the AMR procedure using the classical residual based error estimator (AMRc) without any dual weights . For the Lagrangian method, it is defined as

$$\eta_{classical} = \sqrt{\sum_{T\in\mathcal{T}_h} |\mathbf{r}(T)|^2 + \sum_{F\in\mathcal{F}_h^i} |\mathbf{r}_0(F)|^2 + \sum_{F\in\mathcal{F}_h^b} \Big(|\mathbf{r}_1(F)|^2 + h_F^{-1}\|g-u_h\|_{0,F}^2\Big)},$$

and for Nitsche's method [17], it is defined as

$$\eta_{classical} = \sqrt{\sum_{T\in\mathcal{T}_h} |\mathbf{r}(T)|^2 + \sum_{F\in\mathcal{F}_h^i} |\mathbf{r}_0(F)|^2 + \sum_{F\in\mathcal{F}_h^b} \gamma^2 h_F^{-1}\|g-u_h\|_{0,F}^2}.$$

It is well known that $\eta_{classical}$ is optimal in minimizing the energy norm of the error, i.e., $\|\nabla(u-u_h)\|_{0,\Omega}$. Note that comparing with (2.21), the H^1 norm in $\mathbf{r}_2(F)$ is reduced to L^2 norm on Γ with adjusted weights for the Lagrangian method.

Figure 2 shows the final meshes for the adaptive Lagrangian multiplier method ($k = 2, k' = 0$) using respective $\eta_{classical}$(left) and η(right). It can be seen that the mesh generated by $\eta_{classical}$ has dense refinements around the interior peaks and sinks while the mesh generated by η has more dense refinements near the boundary and almost completely ignores the peaks and sinks in the interior domain.

In the log-log plots Figure 3, we compare the convergence of true errors and estimators. The purpose of the convergence figures is to compare the two adaptive procedures using, respectively, the dual weighted and the classical nonweighted error estimators. From Figure 3(a), we see that the error driven by η converges faster than the one driven by $\eta_{classical}$, which already has the order N^{-1} with N being the total number of DOFs. In comparison with rates attained by uniform refinement, which are provided in the Table 2 and Table 1, the relationship is that the rate obtained by $\eta_{classical}$ is higher than or equal to the uniform approximation rate and that the rate obtained by η is higher than that obtained by $\eta_{classical}$. More in detail, in Figure 3(a) we display two reference straight lines: the slope -1 of the first line refers to the approximation rate in the energy norm that can be attained by the best

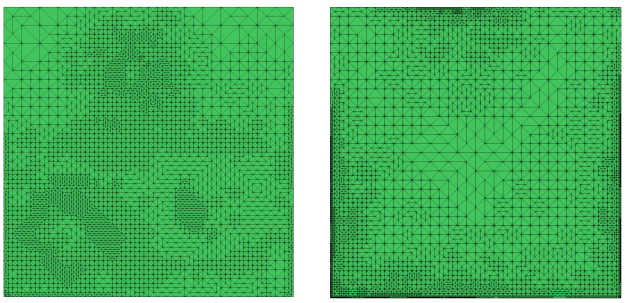

(a) by $\eta_{classical}$ (b) by η

FIG. 2. *Example* 1. *Final meshes for the Lagrangian method* ($k = 2, k' = 0, C_2 = 1.0$).

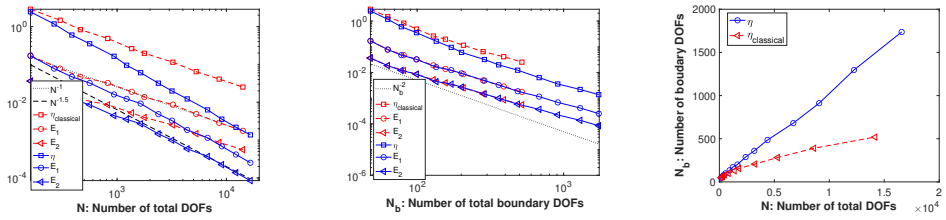

(a) (b) (c)

FIG. 3. *Example* 1. *Convergence comparison for Lagrangian method* ($k = 2, k' = 0, C_2 = 1.0$).

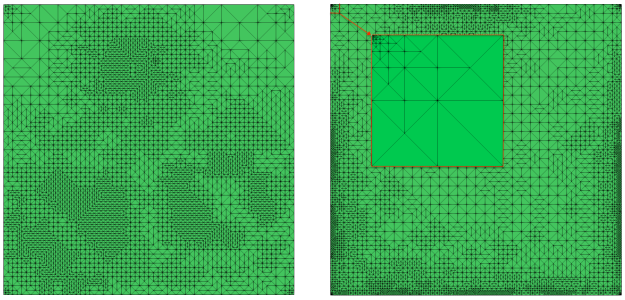

(a) by $\eta_{classical}$ (b) by η

FIG. 4. *Example* 1. *Final meshes for the Lagrangian method* ($k = 2, k' = 2, C_2 = 1$), *including, on the right, a zoom on the upper left corner.*

approximation with order k finite elements on a quasi-uniform grid with N DOFs, which also provides an upper bound for the corresponding error of the normal flux. The slope of the second reference line is numerically evaluated by linear regression of the data set $(\log(N), \log(E))$ from the AMR with the proposed estimator η. For this case its value is ~ -1.5. For the figures thereafter, the same strategies will be used to present the reference slopes.

Figure 3(b) shows that both methods display the same rate of convergence with respect to the number of DOFs on the boundary. However, for the same total number of DOFs, many more DOFs are located on the boundary by η. More precisely, Figure 3(c) shows that the ratio between the number of boundary DOFs and the total DOFs gradually gets higher for the meshes generated by η in the AMR procedure.

We also test Example 1 using the Lagrangian multiplier method with $k = 2$, $k' = 2$, and

$$\Lambda_h = \{\lambda \in C^0(\Gamma) : \ u|_F \in \mathbb{P}_2(F) \ \forall F \in \mathcal{T}_h|_\Gamma\}. \tag{4.4}$$

Since in this test the domain has corners and, consequently, λ is discontinuous, optimal approximation for the multiplier cannot be achieved, as $\lambda_h \in C^0(\Gamma)$. This is also shown in Table 2 for the uniform refinement. In Figure 4(b), we observe that the mesh is densely refined around the corners which indicates that the error estimator η successfully captures the error on the corners. The convergence results of error estimators and the true error are provided in Figure 5, which is similar to Figure 3.

We now test Nitsche's method with $k = 1$ and $k = 2$ and set $\gamma = 10$ in (3.10). Figure 6 compares the final meshes generated using η and $\eta_{classical}$. We observe similar

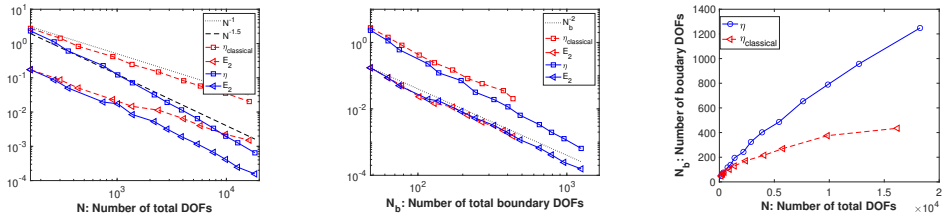

(a) (b) (c)

FIG. 5. *Example* 1. *Convergence comparison for Lagrangian method* ($k = 2, k' = 2, C_2 = 1.0$).

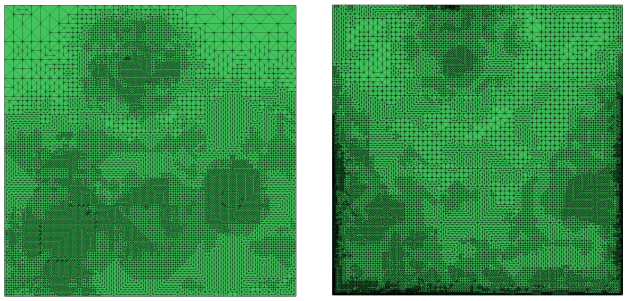

(a) $k = 1$ by $\eta_{classical}$ (b) $k = 1, C_2 = 1.0$ by η

(c) $k = 2$ by $\eta_{classical}$ (d) $k = 2, C_2 = 0.1$ by η

FIG. 6. *Example* 1. *Final meshes for Nitsche's method.*

phenomena to those of the Lagrangian method, i.e., the mesh generated by $\eta_{classical}$ has dense refinement near the interior peaks and sinks, while the mesh generated by η has dense refinements almost all close to the boundary. The corresponding convergence rates of the true error and error estimators are plotted in Figure 7. Again, for both orders, we observe significant improvements of the convergence rate compared to the classical case.

For Nitsche's method of linear order, we also compare the performance with the boundary concentrated meshes proposed in [38] by Pfefferer and Winkler (PW), which yield what is presently the best a priori error estimate for a nonadaptive approximation of the normal flux. The boundary concentrated mesh has a fixed hierarchy structure, i.e., it has uniform mesh size h^2 on the boundary and $h\sqrt{\text{dist}(T,\Gamma)}$ for interior elements. We generate three such meshes in Figure 8.

The corresponding log-log curve of (N, E_2) is plotted with legend $E_{2,PW}$ in Figure 7 (see the top left figure). We observe that the error obtained with this mesh,

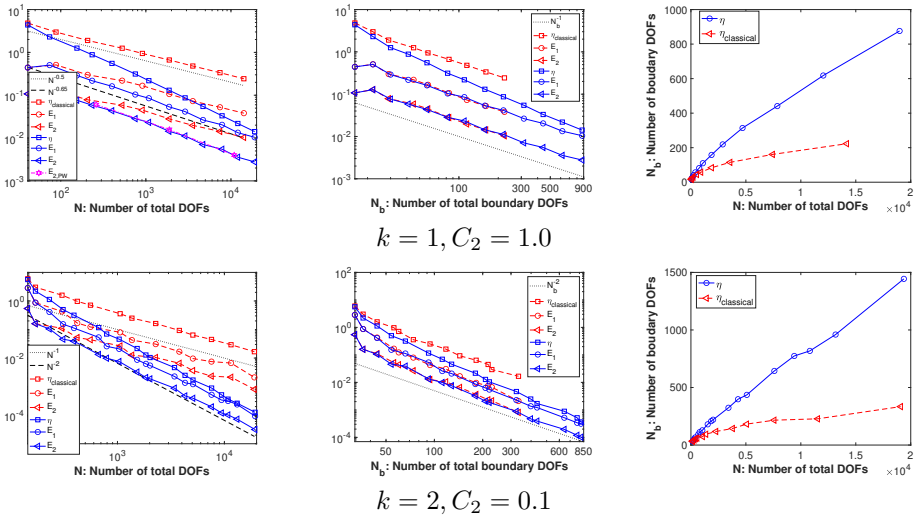

FIG. 7. *Example* 1. *Convergence comparison for Nitsche's method.*

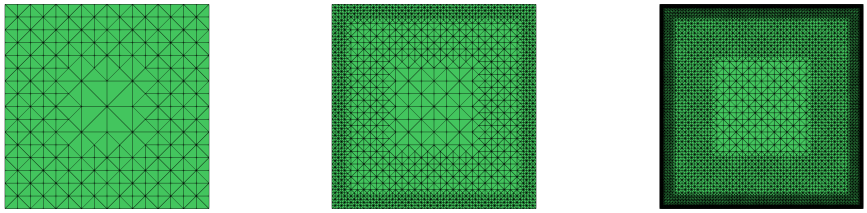

FIG. 8. *Example* 1. *Three meshes for the PW method.*

which is adapted "a priori" to a good approximation of the boundary flux, is very close to the error obtained thanks to our error estimator η. This is not surprising, as the solution of the problem is smooth.

To provide a more complete picture, in Figure 9, we instead compare the performance of the error estimators $\eta_{classical}$ and η, and of the related AMRs, in terms of the convergences in the energy error $\|\nabla(u - u_h)\|_{0,\Omega}$. The results confirm that $\eta_{classical}$ is optimal for the energy error, while, as is to be expected, η yields only a suboptimal rate for the energy error in each of the tests.

Remark that despite the fact that both versions of the Lagrangian method that we tested are, for different reasons, suboptimal with respect to the order k of the bulk discretization, our tests show that the proposed error estimator allows us to obtain a satisfactory approximation of the normal flux also for such methods.

For the remaining examples, to avoid a too large number of redundant tests, we then focus only on Nitsche's method, which is, instead, optimal and which, we recall, is equivalent to the Barbosa–Hughes method. Moreover, we observe that the results displayed before in Table 1 and Figure 7 for Nitsche's method both confirm that E_2 can, after rescaling, serve as a good alternative to the more expensive E_1 in evaluating the true error. As for Nitsche's method with $k = 1$, the ratio E_2/E_1 is stable around 0.25; in the remaining examples, we will use $E = 4E_2$ as the true error.

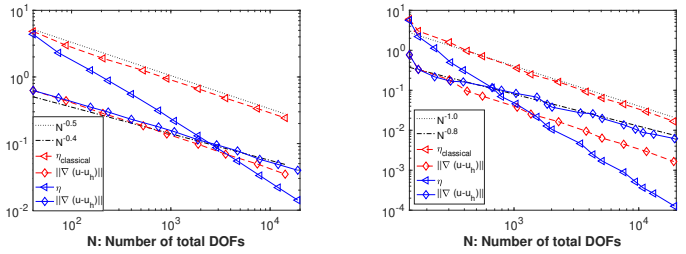

(a) Nitsche $k = 1$ (b) Nitsche $k = 2$

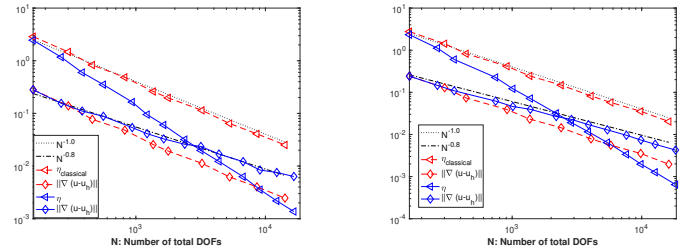

(c) Lagrangian $k = 2, k' = 0$ (d) Lagrangian $k = 2, k' = 2$

FIG. 9. *Example* 1. *Convergence comparison with energy error* $\|\nabla(u - u_h)\|_{0,\Omega}$.

Example 2. In this example, we test a diffusion problem with variable diffusion coefficient. The diffusion coefficient is defined as $a = 1.0 + \sin^2(\pi\sqrt{x^2 + y^2})$. And the functions g and f are defined such that the true solution u has the following representation:

$$u(x, y) = \exp(-\alpha_p((x - x_p)^2 + (y - y_p)^2)) \text{ with } \alpha_p = 200, x_p = 0.2, y_p = 0.2.$$

Note that this function has a strong peak at the point (x_p, y_p).

In the adaptive procedure, the stopping criteria are again set such that the total number of DOFs is less than $20,000$. We test Nitsche's method for both the first and second orders with $C_2 = 1.0$. For Example 2 with variable coefficient, we observe similar numerical behavior as in Example 1; see Figure 10 and Figure 11. From the left two subfigures of Figure 11, we observe that in both cases the convergence rates for the true error using η is almost double that using $\eta_{classical}$. In the example, our adaptive algorithm slightly outperforms the PW method. In the case $k = 2$ we however observe visible oscillations for the true error. This is not in contrast with the theory. Indeed, the Galerkin method minimizes a discrete energy norm of the error which controls the error on the normal flux only up to a constant. Therefore, refining the mesh does not automatically yield a reduction in the error on the normal flux, particularly if measured, as in our case, in a norm that does not depend on the diffusion coefficient a.

Example 3. In this example, we test the L-shaped domain Poisson problem ($a = 1$) with a corner singularity and with an addition interior peak. The true solution has the following representation in polar coordinates:

$$u(r, \vartheta) = r^\alpha \sin(\alpha\vartheta) + \exp(-\alpha_p((x - x_p)^2 + (y - y_p)^2)) \in H^{5/3}(\Omega),$$

where $\alpha = 2/3$, (α_p, x_p, y_p) is the same as in Example 2 and the Ω is the L-shaped domain, i.e., $\Omega = [-1, 1]^2 \setminus (0, 1) \times (-1, 0)$.

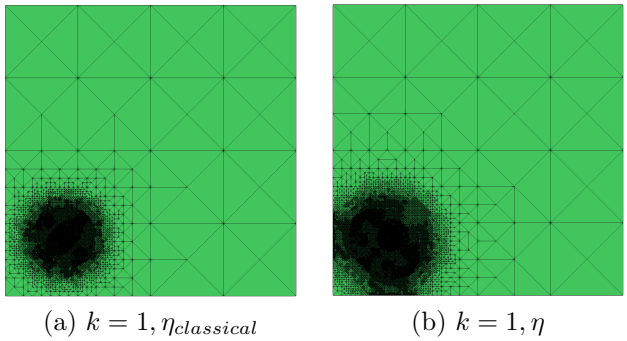

(a) $k = 1, \eta_{classical}$ (b) $k = 1, \eta$

(c) $k = 2, \eta_{classical}$ (d) $k = 2, \eta$

FIG. 10. *Example* 2. *Final meshes for Nitsche's method* ($C_2 = 1.0$).

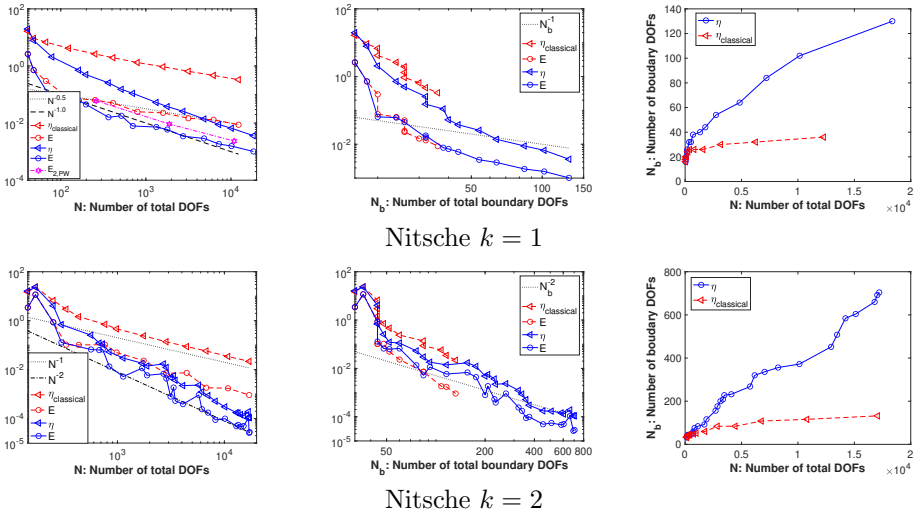

FIG. 11. *Example* 2. *Convergence comparison for Nitsche's method* ($C_2 = 1$).

In this test, we set $C_2 = 1$ and $C_2 = 0.1$ for the first and second order Nitsche's method, respectively. The convergence rate on uniform meshes is firstly verified in Table 3. We recall that, according to the standard a priori error estimates for uniformly refined grids, the error for both the Lagrangian multiplier and Nitsche's method behaves like $h^{5/3-1} = h^{2/3} = N^{-1/3}$.

TABLE 3
Example 3: Convergence rates on uniform meshes.

	Nitsche $k=1$		Nitsche $k=2$	
h	E_2	rate	E_2	rate
1.76E-1	1.10E-2	0.86	6.88E-2	2.53
8.84E-2	1.28E-2	3.10	1.62E-2	2.08
4.42E-2	8.84E-3	0.54	7.93E-3	1.03
2.21E-2	6.04E-3	0.55	5.08E-3	0.64
1.10E-2	4.07E-3	0.56	3.36E-3	0.59
5.52E-3	2.72E-3	0.57	2.23E-3	0.59

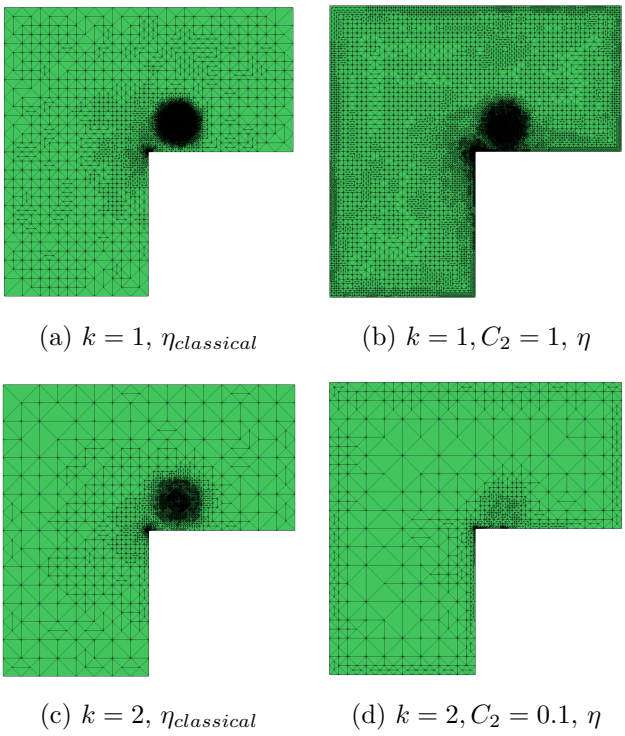

(a) $k=1$, $\eta_{classical}$ (b) $k=1, C_2=1$, η

(c) $k=2$, $\eta_{classical}$ (d) $k=2, C_2=0.1$, η

FIG. 12. *Example 3. Final meshes for Nitsche's method.*

The final meshes obtained for Nitsche's method are given in Figure 12, and the corresponding convergence results are provided in Figure 13. We note that for this problem, even with the low regularity caused by boundary singularity, in both cases the true error E driven by η still doubles the convergence rates with respect to those of $\eta_{classical}$.

In this example, in the presence of the corner singularity on the boundary, the adaptive method based on our error estimator shows significantly better performance than the PW method, which has uniform refinement on the boundary.

Comparing the performance of the estimator in the three examples we see that the adaptive procedure based on the dual weighted residual performs always better than the one based on the classical error estimator. If the solution is smooth, the results obtained by the AMR based on the new estimator are, in terms of error versus number of DOFs, as good as the ones obtained by using boundary concentrated meshes (of course, in this case, this last method is cheaper, as the mesh is designed a priori and

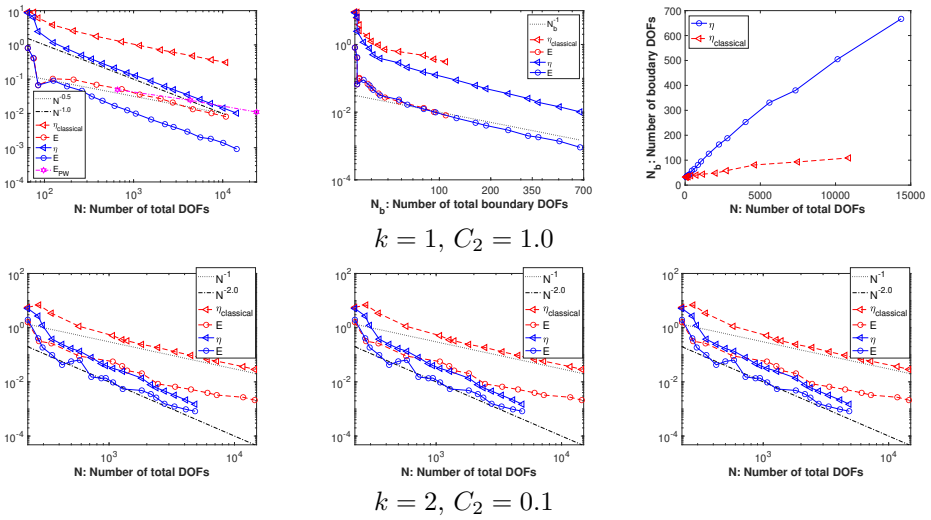

FIG. 13. *Example* 3. *Convergence comparison for Nitsche's method.*

the problem is solved only once). Our adaptive method is particularly advantageous when the solution presents singularities on or close to the boundary (which boundary concentrated meshes, based on a priori analysis, cannot tackle efficiently).

REFERENCES

[1] M. AKIRA, *A mixed finite element method for boundary flux computation*, Comput. Methods Appl. Mech. Engrg., 57 (1986), pp. 239–243, https://doi.org/10.1016/0045-7825(86)90016-2.

[2] T. APEL, J. PFEFFERER, AND A. RÖSCH, *Finite element error estimates on the boundary with application to optimal control*, Math. Comp., 84 (2015), pp. 33–70, https://doi.org/10.1090/S0025-5718-2014-02862-7.

[3] T. APEL, J. PFEFFERER, AND M. WINKLER, *Local mesh refinement for the discretization of Neumann boundary control problems on polyhedra*, Math. Methods Appl. Sci., 39 (2016), pp. 1206–1232, https://doi.org/10.1002/mma.3566.

[4] H. J. C. BARBOSA AND T. J. R. HUGHES, *The finite element method with Lagrange multipliers on the boundary: Circumventing the Babuška-Brezzi condition*, Comput. Methods Appl. Mech. Engrg., 85 (1991), pp. 109–128, https://doi.org/10.1016/0045-7825(91)90125-P.

[5] R. BECKER, E. ESTECAHANDY, AND D. TRUJILLO, *Weighted marking for goal-oriented adaptive finite element methods*, SIAM J. Numer. Anal., 49 (2011), pp. 2451–2469, https://doi.org/10.1137/100794298.

[6] R. BECKER, G. GANTNER, M. INNERBERGER, AND D. PRAETORIUS, *Goal-Oriented Adaptive Finite Element Methods with Optimal Computational Complexity*, preprint, arXiv:2101.11407 [Math.NA], 2021.

[7] R. BECKER, M. INNERBERGER, AND D. PRAETORIUS, *Optimal convergence rates for goal-oriented FEM with quadratic goal functional*, Comput. Methods Appl. Math., 21 (2021), pp. 267–288.

[8] R. BECKER, H. KAPP, AND R. RANNACHER, *Adaptive finite element methods for optimal control of partial differential equations: Basic concept*, SIAM J. Control Optim., 39 (2000), pp. 113–132, https://doi.org/10.1137/S0363012999351097.

[9] R. BECKER AND R. RANNACHER, *A feed-back approach to error control in finite element methods: Basic analysis and examples*, East-West J. Numer. Math., 4 (1996), pp. 237–264.

[10] R. BECKER AND R. RANNACHER, *Weighted A Posteriori Error Control in FE Methods*, Technical report, Universität Heidelberg, 1996.

[11] R. BECKER AND R. RANNACHER, *An optimal control approach to a posteriori error estimation in finite element methods*, Acta Numer., 10 (2001), pp. 1–102, https://doi.org/10.1017/S0962492901000010.

[12] C. Bernardi, Y. Maday, and A. T. Patera, *Domain decomposition by the mortar element method*, in Asymptotic and Numerical Methods for Partial Differential Equations with Critical Parameters, Springer, Cham, 1993, pp. 269–286, https://doi.org/10.1007/978-94-011-1810-1_17.

[13] S. Berrone, A. Bonito, R. Stevenson, and M. Verani, *An optimal adaptive fictitious domain method*, Math. Comp., 88 (2019), pp. 2101–2134, https://doi.org/10.1090/mcom/3414.

[14] S. Bertoluzza, *Local boundary estimates for the Lagrange multiplier discretization of a Dirichlet boundary value problem with application to domain decomposition*, Calcolo, 43 (2006), pp. 121–149, https://doi.org/10.1007/s10092-006-0115-7.

[15] S. Bertoluzza, *Analysis of a mesh-dependent stabilization for the three fields domain decomposition method*, Numer. Math., 133 (2016), pp. 1–36, https://doi.org/10.1007/s00211-015-0742-5.

[16] F. Brezzi, L. P. Franca, D. Marini, and A. Russo, *Stabilization techniques for domain decomposition methods with non-matching grids*, in Proceedings of the Ninth International Conference on Domain Decomposition Methods, P.E. Bjørstad, M.S. Espedal, and D.E. Keyes, eds., 1996, pp. 1–12.

[17] E. Burman, C. He, and M. G. Larson, *A posteriori error estimates with boundary correction for a cut finite element method*, IMA J. Numer. Anal., in press, https://doi.org/10.1093/imanum/draa085.

[18] A. Cohen, I. Daubechies, and J.-C. Feauveau, *Biorthogonal bases of compactly supported wavelets*, Comm. Pure Appl. Math., 45 (1992), pp. 485–560, https://doi.org/10.1002/cpa.3160450502.

[19] W. Dahmen, *Stability of multiscale transformations*, J. Fourier Anal. Appl., 2 (1996), pp. 341–361.

[20] B. H. Dennis and G. S. Dulikravich, *Simultaneous determination of steady temperatures and heat fluxes on surfaces of three dimensional objects using FEM*, in Proceedings of the ASME International Mechanical Congress and Exposition, 2001, pp. 259–268.

[21] K. Eriksson and C. Johnson, *Adaptive finite element methods for parabolic problems.* I. *A linear model problem*, SIAM J. Numer. Anal., 28 (1991), pp. 43–77, https://doi.org/10.1137/0728003.

[22] B. Faermann, *Localization of the Aronszajn-Slobodeckij norm and application to adaptive boundary elements methods. Part* I. *The two-dimensional case*, IMA J. Numer. Anal., 20 (2000), pp. 203–234, https://doi.org/10.1093/IMANUM/20.2.203.

[23] B. Faermann, *Localization of the Aronszajn-Slobodeckij norm and application to adaptive boundary element methods Part* II. *The three-dimensional case*, Numer. Math., 92 (2002), pp. 467–499.

[24] M. Feischl, D. Praetorius, and K. G. van der Zee, *An abstract analysis of optimal goal-oriented adaptivity*, SIAM J. Numer. Anal., 54 (2016), pp. 1423–1448, https://doi.org/10.1137/15M1021982.

[25] R. Franke, *A Critical Comparison of Some Methods for Interpolation of Scattered Data*, Technical report, Naval Postgraduate School, Monterey, CA, 1979.

[26] D. Gilbarg and N. S. Trudinger, *Elliptic Partial Differential Equations of Second Order*, Classics in Mathematics, Springer-Verlag, Berlin, 2001.

[27] M. B. Giles, M. G. Larson, M. Levenstam, and E. Süli, *Adaptive Error Control for Finite Element Approximations of the Lift and Drag Coefficients in Viscous Flow*, Manuscript, 1997.

[28] V. Girault and R. Glowinski, *Error analysis of a fictitious domain method applied to a Dirichlet problem*, Jpn. J. Ind. Appl. Math., 12 (1995), pp. 487–514, https://doi.org/10.1007/BF03167240.

[29] P. M. Gresho, R. L. Lee, R. L. Sani, M. K. Maslanik, and B. E. Eaton, *The consistent Galerkin FEM for computing derived boundary quantities in thermal and or fluids problems*, Internat. J. Numer. Methods Fluids, 7 (1987), pp. 371–394, https://doi.org/10.1002/fld.1650070406.

[30] M. Holst and S. Pollock, *Convergence of goal-oriented adaptive finite element methods for nonsymmetric problems*, Numer. Methods Partial Differential Equations, 32 (2016), pp. 479–509, https://doi.org/10.1002/num.22002.

[31] M. Holst, S. Pollock, and Y. Zhu, *Convergence of goal-oriented adaptive finite element methods for semilinear problems*, Comput. Vis. Sci., 17 (2015), pp. 43–63, https://doi.org/10.1007/s00791-015-0243-1.

[32] T. Horger, J. M. Melenk, and B. Wohlmuth, *On optimal L2- and surface flux convergence in FEM*, Comput. Vis. Sci., 16 (2013), pp. 231–246, https://doi.org/10.1007/s00791-015-0237-z.

[33] M. Innerberger and D. Praetorius, *Instance-optimal goal-oriented adaptivity*, Comput. Methods Appl. Math., 21 (2021), pp. 109–126, https://doi.org/10.1515/cmam-2019-0115.
[34] B. Khoromskij and J. Melenk, *Boundary concentrated finite element methods*, SIAM J. Numer. Anal., 41 (2004), pp. 1–36.
[35] M. G. Larson and A. Massing, *L^2-Error Estimates for Finite Element Approximations of Boundary Fluxes*, preprint, arXiv:1401.6994 [Math.NA], 2014.
[36] J. Nerg and J. Partanen, *A simplified FEM based calculation model for 3-D induction heating problems using surface impedance formulations*, IEEE Trans. Magn., 37 (2001), pp. 3719–3722, https://doi.org/10.1109/20.952698.
[37] J. Nitsche, *Über ein variationsprinzip zur lösung von Dirichlet-problemen bei verwendung von teilräumen, die keinen randbedingungen unterworfen sind*, Abh. Math. Semin. Univ. Hambg., 36 (1971), pp. 9–15.
[38] J. Pfefferer and M. Winkler, *Finite element error estimates for normal derivatives on boundary concentrated meshes*, SIAM J. Numer. Anal., 57 (2019), pp. 2043–2073, https://doi.org/10.1137/18M1181341.
[39] T. Richter and T. Wick, *Variational localizations of the dual weighted residual estimator*, J. Comput. Appl. Math., 279 (2015), pp. 192–208, https://doi.org/10.1016/j.cam.2014.11.008.
[40] L. R. Scott and S. Zhang, *Finite element interpolation of nonsmooth functions satisfying boundary conditions*, Math. Comp., 54 (1990), pp. 483–493, https://doi.org/10.2307/2008497.
[41] R. Stenberg, *On some techniques for approximating boundary conditions in the finite element method*, J. Comput. Appl. Math., 63 (1995), pp. 139–148, https://doi.org/10.1016/0377-0427(95)00057-7.
[42] A. Veeser and R. Verfürth, *Poincaré constants for finite element stars*, IMA J. Numer. Anal., 32 (2011), pp. 30–47, https://doi.org/10.1093/imanum/drr011.